ACS Macro Letters

Letter

pubs.acs.org/macroletters

Plastic Deformation Mechanisms of Semicrystalline and Amorphous Polymers

Sara Jabbari-Farouji,*[,†] Joerg Rottler,[‡] Olivier Lame,[§] Ali Makke,[∥] Michel Perez,[§] and Jean-Louis Barrat[†,⊥]

[†]Université Grenoble Alpes, UJF Liphy, F38041 Grenoble, France

[‡]Department of Physics and Astronomy, The University of British Columbia, 6224 Agricultural Road, Vancouver, British Columbia V6T 1Z1, Canada

[§]INSA Lyon, MATEIS, UMR CNRS 5510, Université de Lyon, F69621 Villeurbanne, France

[∥]EPF école d'ingénieur, Institut Charles Delaunay, LASMIS UMR CNRS 6279, F10004 Troyes, France

[⊥]Institut Laue-Langevin, 6 rue Jules Horowitz, BP 156, F-38042 Grenoble, France

ABSTRACT: We use large-scale molecular dynamics simulations to investigate plastic deformation of semicrystalline polymers with randomly nucleated crystallites. The strain-softening regime is dominated by deformation of crystallites via reorientation of chain-folded lamellae toward the tensile axis, fragmentation of largest crystalline domains, and a partial loss of crystallinity. The strain-hardening regime coincides with unfolding of chains and recrystallization as a result of strain-induced chain alignment. These observed deformation mechanisms are consistent with experimental findings. We compare the tensile behavior of semicrystalline polymers with their amorphous counterparts at temperatures above and below the glass transition temperature.

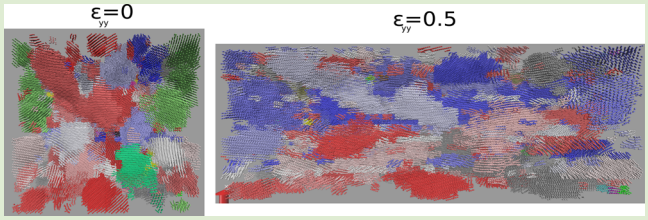

Deformation mechanisms in the plastic flow regime of amorphous polymers (either rubbery or glassy) have been widely investigated[1−5] and are rather well understood. However, the underlying mechanisms of deformation in their semicrystalline counterparts are still controversial.[6,7] Under stretching, semicrystalline polymers undergo a complete molecular rearrangement of the chain-folded lamellae, typically of isotropic spherulitic morphology, into a highly oriented chain-unfolded fibrillar microstructure at high strains. It has been suggested that yielding is controlled by nucleation and the motion of screw dislocations in the crystalline domains,[8] and it depends on density of stress transmitters.[9] The crystallographic slip mechanisms within the lamellae are thought to be an active deformation mechanism at all strain levels.[6] At large deformations, strain-induced melting and recrystallization processes have been proposed to be the dominant mechanism of the structure transformation[10] as confirmed by recent experiments.[11]

Because of the small length scales involved, it is not possible to observe experimentally local mechanisms of plastic deformation and to disentangle the deformations in ordered and amorphous parts. The few simulations that exist on this matter[12,13] focus on deformation of a stacked lamellar configuration which mimics a small part of the spherulite structure. Our aim is to fill this gap by performing large-scale molecular dynamics simulations of semicrystalline polymers and by analyzing the evolution of polymer conformations and crystalline domains along the stress−strain curve. We employ a coarse-grained model representing polyvinyl alcohol (CG-PVA).[14] By changing the cooling rate, we can tune the degree of crystallinity and observe both crystallization and glass formation. The semicrystalline samples obtained by this method are dominated by homogeneous nucleation and correspond to a microstructure of randomly oriented small crystallites (<100 nm) in contrast to the spherulitic structures with a lateral size of a few micrometers. Nevertheless, it is remarkable that the CG-PVA model reproduces most of the mechanical behavior of real semicrystalline polymers.

Molecular dynamics simulations of the CG-PVA model[14] were carried out using LAMMPS[17] of systems up to 4.3×10^6 monomers obtained from replications of smaller samples (9×10^4 monomers). The chain length is set to $N = 300$, which corresponds roughly to 9−10 entanglement lengths as determined by Primitive-Path Analysis.[16] Distances are reported in length units $\sigma = 0.52$ nm, and the bond length is $b_0 = 0.5\sigma$. The range and strength of 6-9 Lennard-Jones potential for nonbonded interactions are given by $\sigma_{LJ} = 0.89\sigma$ and $\varepsilon_{LJ} = 1.511 k_B T_0$ where $T_0 = 550$ K is the reference temperature of the PVA melt.[14] The Lennard-Jones potential is truncated and shifted at $r^c_{LJ} = 1.6\sigma$. The time unit from the conversion relation of units is $\tau = 1.31$ ps, and the temperatures and pressures are reported in reduced units $T = T_{real}/T_0$ and $P = P_{real}\sigma^3/\varepsilon_0$. We apply periodic boundary conditions in the NPT ensemble using a Berendsen barostat ($P = 8$) and a Nose-Hoover thermostat. The time step in our simulations is 0.005τ.

Received: November 30, 2014
Accepted: January 5, 2015
Published: January 14, 2015

DOI: 10.1021/mz500754b
ACS Macro Lett. 2015, 4, 147−150

To characterize the crystallites, we use the notion of crystalline domains which are defined as a set of spatially connected regions with the same orientation.[18] To identify the crystalline domains, we divide the box into cells of size about 2σ, and we compute the nematic tensor $Q_{\alpha\beta} = 1/N\sum_t(3/2b^i_\alpha b^i_\beta - 1/2\delta_{\alpha\beta})$ of unit bond vectors of polymers $\hat{b}^i$ within each cell. The largest eigenvalue and the corresponding eigenvector of the nematic tensor determine the order parameter S and the preferred orientation of bonds, i.e., director $\hat{n}$ in each cell. The volume fraction of cells with $S > 0.8$ defines the degree of crystallinity X_C. We perform a cluster analysis by merging two neighboring cells if they are both crystalline, and their directors share the same orientation within the threshold $\hat{n}\cdot\hat{n}' \geq 0.97$. We determine the volume distribution of crystallites as a function of $V_{\text{domain}} = nv_{\text{cell}}$ where n is the number of cells with volume v_{cell} in a domain, and we normalize it to the volume of the box V. Thus, we obtain $(d\Phi/dV) = [(nv_{\text{cell}}N(n))/(V\Delta n)]$ where $N(n)$ is the number of domains which comprise between n and $n + \Delta n$ crystalline cells.

Equilibrated melts at density $\rho\sigma^3 = 2.35$ at $T = 1$ are cooled to the desired temperature with cooling rates in the range $2 \times 10^{-7} < \dot{T} < 10^{-3}\tau^{-1}$ as presented in Figure 1. For $\dot{T} \leq 10^{-5}\tau^{-1}$,

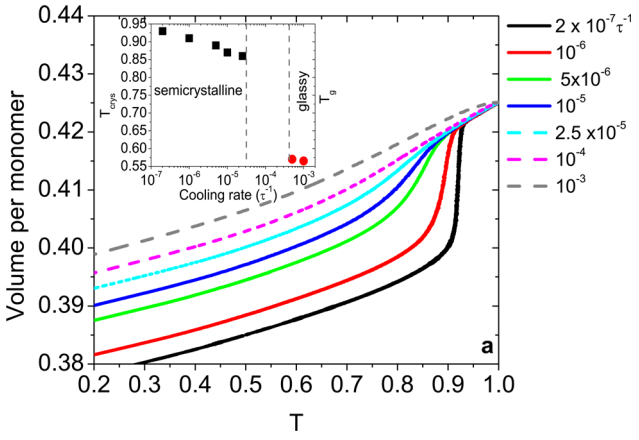

Figure 1. Volume per monomer v as a function of T for 3600 chains of 300 monomers obtained at different reduced cooling rates $\dot{T}$. The inset shows T_{crys} (black squares) and T_g (red discs) versus $\dot{T}$.

we observe an abrupt change of volume and slope of the $v-T$ curve around a certain temperature. These sharp changes are attributed to the partial crystallization of polymers,[14,15] and the temperature marking these changes defines the crystallization temperature T_{crys}. For faster cooling rates, the slope changes of $v-T$ curves are less abrupt, and the polymers retain their amorphous configurations during cooling. The system undergoes a glass transition, and the temperature at which the slope of the cooling curve changes gives us an estimation of the glass transition temperature T_g. The inset of Figure 1 shows T_{crys} and T_g as a function of cooling rate. Note that T_g can only be defined for the samples obtained with the fastest cooling rates, when the crystallinity vanishes even at the lowest temperatures.

We now turn to the mechanical response of polymers under uniaxial tension. In tensile tests, the samples are deformed in the y-direction with a constant true strain rate of $10^{-5}\tau^{-1}$, and a pressure of $P = 8$ (the same pressure as the nondeformed sample[14]) is imposed in the x- and z-directions. Concomitant with stretching of the box in the tensile direction, the samples shrink in the perpendicular directions. The volume increase is at most 6% for the semicrystalline polymers at lowest temperature $T = 0.2$, while for the amorphous polymers, the volume increase is less than 2% at all T. Therefore, PVA polymers behave nearly as an incompressible fluid.

Figure 2a and Figure 2b present the stress–strain curves obtained for different crystallinities at two temperatures above and below the glass transition temperature, i.e., $T = 0.7$ and $T = 0.2$. In all samples, we observe an elastic regime at low deformations and a strain-hardening regime at very large deformations. The elastic regime of deformation is followed by an overshoot typical of yield-stress fluids for semicrystalline polymers and low-temperature amorphous samples. We define the yield-stress σ_y as the maximum value of stress in the overshoot region. We have plotted σ_y against crystallinity at each temperature in the insets of Figure 2a and Figure 2b. Young's modulus E is extracted from the linear response regime.

At $T = 0.7 > T_g$, where the amorphous part is in the rubbery state, E and σ_y rise strongly upon increase of crystallinity, presumably due to formation of a percolating crystalline network. Samples with largest crystallinity exhibit a stress plateau before entering the strain-hardening regime. At $T = 0.2 < T_g$, where the amorphous part is glassy, we find that all the samples are stiffer than their high-temperature counterparts, and E shows a similar trend as at $T = 0.7$. Interestingly, σ_y is a nonmonotonic function of crystallinity and has the lowest value

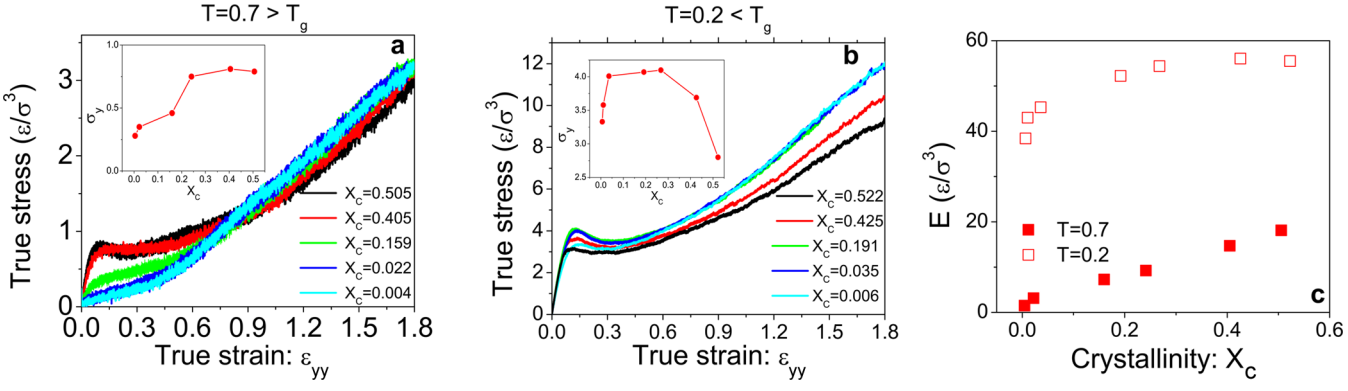

Figure 2. Stress–strain curves obtained from uniaxial tensile tests at (a) $T = 0.7$ and (b) $T = 0.2$ for different crystallinities. The corresponding X_C values are shown in the legends, and the cooling rates from the highest to the lowest crystallinity correspond to $2 \times 10^{-7}\tau^{-1}$, $10^{-6}\tau^{-1}$, $10^{-5}\tau^{-1}$, $10^{-4}\tau^{-1}$, and $10^{-3}\tau^{-1}$, respectively. (c) Young modulus E versus X_C. Here, $\varepsilon/\sigma^3 \approx 54$ MPa.

DOI: 10.1021/mz500754b
ACS Macro Lett. 2015, 4, 147–150

at the highest X_C. Furthermore, all the samples show a strain-softening regime.

Next, we focus on the mechanisms of plastic deformation beyond the yield point, i.e., the strain-softening and strain-hardening. Figure 3 shows the conformation of semicrystalline

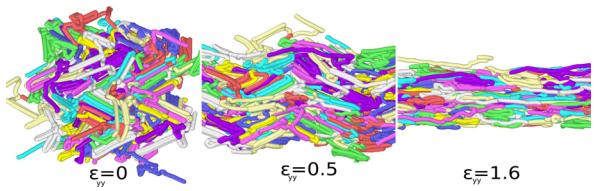

Figure 3. Snapshots of semicrystalline polymers at $T = 0.2$ obtained for $X_C = 0.425$ at different stages of deformation.

polymers at different stages of plastic deformation. At strains beyond the yield point, the chain-folded structures align partially in the direction of tensile stress. At larger deformations in the strain-hardening regime, chains in crystalline domains are unfolded as a result of tensile stress, and both chains in amorphous and crystalline domains are stretched and aligned.

To quantify our visual observations, we characterize the volume fraction distribution of crystalline domains $d\Phi/dV$ (Figure 4), crystallinity X_C, and global nematic order parameter S_{global} (Figure 5) upon increase of deformation. In the plastic flow region, we recognize the following regimes:

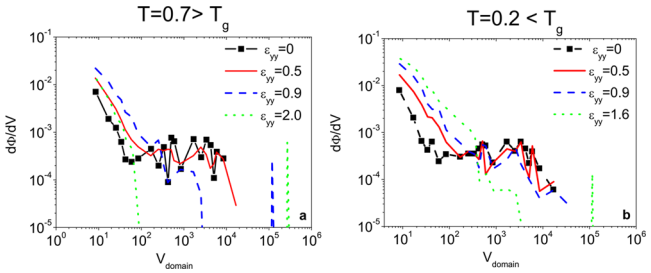

Figure 4. Volume distribution function of crystalline domains $d\Phi/dV$ in semicrystalline samples obtained for $X_C = 0.425$ at (a) $T = 0.7$ and (b) $T = 0.2$ at different strains.

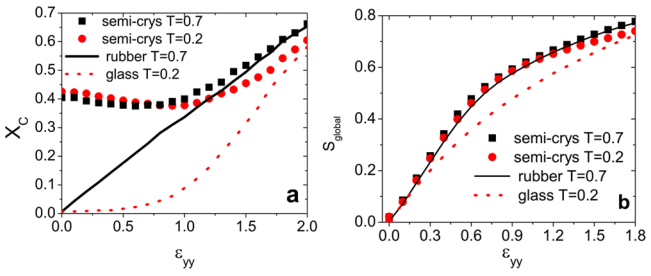

Figure 5. (a) Crystallinity and (b) the global nematic order parameter S_{global} for the semicrystalline sample obtained at $X_C = 0.425$ and amorphous polymers.

Strain softening/stress plateau regime: coincides with strains in the range $0.1 < \varepsilon_{yy} < 0.75$ for $T = 0.7$ and $0.1 < \varepsilon_{yy} < 1.1$ for $T = 0.2$. Figure 4 reveals that the volume fraction of the largest crystalline domains decreases and that of the smallest ones increases. This implies fragmentation of the larger crystalline domains that leads to a partial loss of crystallinity as also evidenced by Figure 5a. We also find that the population of bonds along the tensile axis in both ordered and disordered regions increases although reorientation is dominated by the bonds in the crystalline regions. By examining pair distribution functions (not shown) in the direction perpendicular to the tensile deformation, we recognize a correlation between the rotation of crystallites and the decrease of nearest neighbor distance between nonbonded monomers in the perpendicular direction in the crystalline regions. These observations lead us to conclude that the strain softening/plateau regime is dominated by reorientation of crystallites in the direction of tensile axis and fragmentation of some of the larger crystalline domains.

Strain hardening regime: corresponds to $\varepsilon_{yy} > 0.7$ ($T = 0.7$) and $\varepsilon_{yy} > 1.1$ ($T = 0.2$). This regime is delineated by the onset of an increase in X_C. It results from alignment of chains as evidenced by $S_{global} > 0.5$ (Figure 5b). Notably, the volume distribution of crystalline domains in Figure 4 changes dramatically at such large strains. $d\Phi/dV$ comprises a set of small domains and a large domain of aligned chains. Chains both in crystalline and disordered parts align along the tensile axis as verified by inspection of pair distribution functions. Hence, a majority of chains contribute to formation of a large crystalline domain.

We finally discuss changes of conformation of amorphous polymers under tensile deformation as presented in Figure 2. At $T = 0.7$ where the polymers are in the rubbery state, we observe a crossover from an elastic regime of purely entropic origin[1] to the strain-hardening regime at $\varepsilon_{yy} \approx 0.45$. Strain hardening occurs when chains align with the tensile axis and $S_{global} > 0.4$ (Figure 5b).[1] At $T = 0.2$, glassy polymers show a markedly different tensile response from their amorphous counterparts at $T = 0.7$. We observe a strain-softening regime similar to semicrystalline polymers although the origin of yielding is different and results from overcoming free energy barriers.[4,5] Similar to rubbery polymers, the onset of strain hardening corresponds to $S_{global} > 0.4$, and it is accompanied by a strain-induced crystallization (Figure 5a) at large deformations. The strain hardening is shown to be related to the work needed to reorient the chains along the tensile axis.[4,5]

Comparing our simulations with experiments, we notice some differences that are due to limitations in the simulations and the coarse-grained nature of the polymer model. Indeed, to crystallize in an accessible number of MD steps, it is necessary to use a rapidly crystallizable model like CG-PVA. The reduced cooling rates in simulations correspond to 8.4×10^7 K s^{-1} $< \dot{T} <$ 4.2×10^{11} K s^{-1} and are much faster than the most rapid cooling rates in experiments. A high number of nuclei appear in a relatively small number of MD steps for the slowest cooling rate. As a result, the semicrystalline microstructures differ from the classical spherulitic structures observed in real polymers. Nonetheless, it is striking that most of the obtained trends qualitatively agree with the main features of semicrystalline polymers. More quantitatively, the Young modulus values for temperatures above and below $T_g \approx 320$, $E(T = 0.7 \equiv 385\ \text{K}) \approx 0.8$ GPa and $E(T = 0.2 \equiv 110\ \text{K}) \approx 3$ GPa, are comparable to the values reported for PVA polymers.[21] The yielding occurs at strains of about 10% which is consistent with typical values from polymers.[11]

The plastic deformation mechanisms observed in our simulations are also in line with experimental findings. For $T > T_g$ where the amorphous phase is in the rubbery state, the model clearly captures the increase of E and σ_y as a function of crystallinity. In terms of microstructure evolution during deformation, this model accounts for the progressive fracture

DOI: 10.1021/mz500754b
ACS Macro Lett. 2015, 4, 147−150

of the larger crystallites to obtain smaller ones in the stress-plateau regime. The existence of a crystalline network and the predominant deformation of crystalline domains in the stress-plateau regime are in accordance with experiments where semicrystalline polymers are found to behave as two interpenetrated networks of a hard crystalline skeleton and an entangled amorphous phase.[19,20] Thus, at relatively small deformations, the hard crystalline skeleton dominates, whereas the entangled amorphous network is predominant in the strain-hardening regime as amorphous polymers reorient along the tensile axis. The additional crystallinity observed at large deformations beyond the melting/recrystallization process[10,11,22,23] is due to alignment of amorphous chains and is also observed for amorphous polymers in Figure 5a. This explains the stronger strain-hardening behavior for fully amorphous polymers. For the low-temperature case $T < T_g$ where the amorphous phase is in the glassy state, the stress−strain curves as well as the evolution of E with crystallinity agree with the experimental trends. Here, we also observe reorientation and fragmentation of crystallites in the strain-softening regime similar to the plateau regime of the $T > T_g$ sample. However, it seems that the amorphous glassy network also plays a role in plastic deformation as the yield stress of purely amorphous polymers is higher than that of semicrystalline polymers with the highest X_C. Indeed, the strain−stress curves for glass and semicrystalline polymers are quite similar. Hence, as strain softening only exists for low-temperature samples, it is most probably correlated with yielding of glassy regions. The nonmonotonic behavior of σ_y versus crystallinity has so far not been observed and raises interesting open questions about the interplay between plasticity of glassy and crystalline regions operative at the yield point.

In conclusion, simulations of coarse-grained semicrystalline polymers allow us to observe directly the mechanisms of plastic deformation at length scales smaller than 100 nm which are not accessible by experiments. The similarity of plastic deformation mechanisms and trends for a very disordered arrangement of crystallites in our simulations and the experimental structures demonstrates that the spherulitic structure is not the main feature that generates the dominant mechanical features of semicrystalline polymers, and the underlying lamella at smaller length scales dominate the mechanical properties.

AUTHOR INFORMATION

Corresponding Author

*E-mail: sara.jabbari@gmail.com.

Notes

The authors declare no competing financial interest.

ACKNOWLEDGMENTS

We are grateful to H. Meyer for providing the LAMMPS scripts and useful discussions. All of the computations presented in this paper were performed using the Froggy platform of the CIMENT infrastructure (https://ciment.ujf-grenoble.fr), which is supported by the Rhône-Alpes region (GRANT CPER07-13 CIRA) and the Equip@Meso project (reference ANR-10-EQPX-29-01) of the programme Investissements d'Avenir supervised by the Agence Nationale pour la Recherche. JLB is supported by Institut Universitaire de France and by grant ERC-2011-ADG20110209.

REFERENCES

(1) Treloar, L. R. G. *The Physics of Rubber Elasticity*; Clarendon Press: Oxford, 1975.
(2) Haward, R. N.; Young, R. *J. in The Physics of Glassy Polymers*, 2nd ed.; Chapman and Hall: London, 1997.
(3) Strobl, G. *The Physics of Polymers*, 3rd ed.; Springer: Berlin, 2007.
(4) Hoy, R. S.; Robbins, M. O. *J. Polym. Sci., Part B: Polym. Phys.* **2006**, *44*, 3487−3500.
(5) Hoy, R. S.; Robbins, M. O. *Phys. Rev. E* **2008**, *77*, 031801.
(6) Bartczak, Z.; Galeski, A. *Macromol. Symp.* **2010**, *294-I*, 67−90.
(7) Oleinik, E. F.; Rudnev, S. N.; Salamatina, O. B. *Polym. Sci. A* **2007**, *49*, 1302−1327.
(8) Young, R. J. *Philos. Mag.* **1976**, *30*, 86−94.
(9) Humbert, S.; Lame, O.; Vigier, G. *Polymer* **2009**, *50* (15), 3755−3761.
(10) Flory, P. J.; Yoon, D. Y. *Nature* **1978**, *272*, 226−229.
(11) Wang, Y.; Jiang, Z.; Wu, Z.; Men, Y. *Macromolecules* **2013**, *46*, 518522.
(12) Lee, S.; Rutledge, G. C. *Macromolecules* **2011**, *44*, 3096−3108.
(13) In't Veld, P. J.; Hätter, M.; Rutledge, G. C. *Macromolecules* **2006**, *39*, 439−447.
(14) Meyer, H.; Müller-Plathe, F. *J. Chem. Phys.* **2001**, *115*, 7807.
(15) Meyer, H.; Müller-Plathe, F. *Macromolecules* **2002**, *35*, 1241−1252.
(16) Everaers, R.; Sukumaran, S. K.; Grest, G. S.; Svaneborg, C.; Sivasubramanian, A.; Kremer, K. *Science* **2004**, *303*, 823−826.
(17) Plimpton, S. *J. Comput. Phys.* **1995**, *117*, 1.
(18) Luo, C.; Sommer, J.-U. *J. Polym. Sci., Part B: Polym. Phys.* **2010**, *48*, 2222−2232.
(19) Men, Y.; Rieger, J.; Strobl, G. *Phys. Rev. Lett.* **2003**, *91* (9), 095502.
(20) Sun, Y.; Fu, L.; Wu, Z.; Men, Y. *Macromolecules* **2013**, *46* (3), 971−976.
(21) Tokita, N.; Kawai, H. *J. Phys. Soc. Jpn.* **1951**, *6*, 367−371.
(22) Butler, M. F.; Donald, A. M.; Bras, W.; Mant, G. R.; Derbyshire, G. E.; Ryan, A. J. *Macromolecules* **1995**, *28*, 638393.
(23) Jiang, Z.; Tang, Y.; Rieger, J.; Enderle, H. F.; Lilge, D.; Roth, S. V.; et al. *Macromolecules* **2010**, *43*, 472732.

DOI: 10.1021/mz500754b
ACS Macro Lett. 2015, 4, 147−150